Characterization and tribological behavior of TiAlN/TiAlCN multilayer coatings

Zhefeng Lei,[1,2] Xiaodong Zhu,[2] Yanhuai Li,[2] Zhongxiao Song,[2,*] Haiping Liu,[1,*]

Yong Qing Fu[3]

1 Xi'an Aviation Brake Technology Co., Ltd., Xi'an, Shaanxi, 710075, China

2 State Key Laboratory for Mechanical Behavior of Materials, School of Materials Science and Engineering, Xi'an Jiaotong University, Xi'an, Shaanxi, 710049, China

3 Faculty of Engineering and Environment, Northumbria University, Newcastle upon Tyne, NE1 8ST, UK

Abstract

Effects of partial pressure of methane on deposition rate, hardness, bonding strength and friction coefficient of TiAlN/$TiAlC_{0.37}N_{0.63}$ multilayer coating were investigated. The TiAlN coating was deposited at a N_2 flow rate of 70 sccm, and $TiAlC_{0.37}N_{0.63}$ coating were deposited at a N_2 flow rate of 35 sccm and a CH_4 flow rate of 35 sccm. TiAlN/$TiAlC_{0.37}N_{0.63}$ multilayer coatings with different modulation periods but the same total thickness of 3.56 μm were deposited on high speed steel substrates using multi-arc ion plating technology. Microhardness and tribological measurement show that the multilayer coating with a modulating ratio of 1:1 and a modulation period of 68 nm had a hardness of 2793.9 $HV_{0.10}$, an excellent bonding strength of 52N and the

*Corresponding author. E-mail addresses: ZhongxiaoSong@mail.xjtu.edu.cn (Z. Song), llhhpp198123@126.com(H. Liu)

minimum friction coefficient of 0.46 and a relatively low wear rate.

Keywords:

TiAlCN, multilayer, nanoindentation, friction and wear behavior,

1. Introduction

Hard coatings are crucial for technological advances in the fields of modern precision machining[1, 2]. Being one of the mostly used hard coatings, TiAlN has been widely used on the surfaces of metal cutting tools[3-6]. In recent years, much research work has been focused on increasing film modulus and hardness, and improving the coating toughness, wear, friction properties using various multi-component or composite coatings, such as TiAlCN[7], TiAlZrN [8], TiAlSiN [9], TiSiVN [10]. Using these nanocomposite design methodology, coating hardness and toughness could be improved substantially owing to the solid solution strengthening effect. As a matter of fact, nanocomposite coating design has been widely applied to improve the toughness, adhesion, mechanical and tribological properties[11-13]. Furthermore, multilayer coating designs composed of sub-layers in nanometer scales were also developed to improve performance under the dry machining because the multiple and nanoscale interfaces could inhibit the propagation of cracks, lower the residual stress, increase the adhesion strength as well as hardness, with example including TiAlN/VN[14], TiAlN/TiN[15], TiAlN/Ta[16] and TiAlN/SiN[17].

Carbon doped TiAlN coatings or TiAlCN coating, has also been frequently reported[18, 19]. For carbon-doped TiAlN coatings, the structure changed from NaCl-type phase to a nano-composite structure with increasing C content, and the friction coefficient decreased from 0.8 to 0.19 when the C content reached 26.69 at.%. [20] However, the film is very brittle and the toughness is not good. In order to improve this, multilayer design has been proposed in this work. As far as we have known,

there is no previous report on this multilayer design. In this study, TiAlN/TiAlCN multilayer coatings were deposited using multi-arc ion plating, and their morphological, chemical states, mechanical and tribological properties have been characterized.

2. Experimental details

High speed steel (HSS, W6Mo5Cr4V2) of 30×30×4 mm in size was used as the substrate. Before deposition, the substrates were polished and cleaned in an ultrasonic bath with acetone, ethanol and deionized water for 10 min, respectively. Prior deposition, the substrates were plasma cleaned in a deposition chamber using Ar+ bombardment with a bias voltage of 800 V. TiAlN, TiAlCN and multilayer TiAlN/TiAlCN coatings were deposited on the substrates using multi-arc ion plating method. TiAl alloy (50 at.% of aluminum and 50 at.% of titanium) targets with 62 mm in diameter was used and the chamber is a cylinder (700 mm in height and 900 mm in diameter). The substrates were mounted on a rotational holder positioned at the center of the chamber. The distance between the target and the substrate was 300 mm, and the substrate holder was rotated at a speed of 7 rpm.

The deposition was conducted under a negative bias of -100 V with a duty cycle of 30% at a substrate temperature of 573 K, and the deposition pressure was 1.2~1.7 Pa. The DC arc sources were operated at current of 85 A and voltage of 17.3 V for the TiAl target. For single-layer coating, the working gas was a mixture of argon, nitrogen and methane, and the flow rates of Ar, N_2 and CH_4 are listed in Table 1, the duration

of film deposition was 150 min. For the TiAlN/TiAlCN multilayer coatings, the TiAlN sub-layer was deposited in the work atmosphere of Ar (12 sccm) and N_2 (70 sccm), and the TiAlCN sub-layer was deposited in Ar (12 sccm), N_2 (35 sccm) and CH_4 (35 sccm). The layer thicknesses in the thin films were controlled by deposition time. Table 2 lists the deposition parameters for multilayer TiAlN/$TiAlC_{0.37}N_{0.63}$ coatings. Three different layer thickness designs have been used: (1) TiAlN for 1 min and TiAlCN for 1 min; (2) TiAlN for 2 min and TiAlCN for 1 min; (3) TiAlN for 3 min and TiAlCN for 1 min. To get clear interface, when the deposition completed for each sub-layer, the target sources and gas valves should be closed, and after reaching of the setting of vacuum, the next sub-layer should be deposited. In order to improve the coating adhesion, 50 nm TiAl buffer layer and 150 nm TiAlN transition layer were deposited firstly. A TiAlCN capping layer of 350 nm thick was deposited as the top layer for all the cases.

Surface and cross-section morphologies were characterized using a scanning electron microscope (SEM, FEI Quanta 600 FEG). Crystalline structures and phases of the coatings were analyzed using X-ray diffraction (XRD) with a Cu Kα radiation (0.15418 nm). X-ray photoelectron spectroscopy (XPS) was used to analyze the element content and chemical states in $TiAlC_xN_{1-x}$ coatings. Hardness of the single-layer and multilayer coatings was obtained using Nano Indenter and Vickers microhardness instrument, respectively. Adhesion of the coating was evaluated using scratch tests (WS-2005) with a Vickers Indenter together with an acoustic signal monitor. Tribological properties were studied using a ball-on-disk wear tester with a

load of 3N and a ball with a diameter of 3 mm, The rotational speed was 10 cycle per second. The wear counterparts Si_3N_4 balls had a surface roughness (Ra) of 0.02 μm. The wear rate was tested by means of profilometer, and the results only reflect the information about the cleaned coating surface after the wear test. All the measurement value was obtained from the arithmetic average value for each specimen, and the measurement was repeated at least 5 measurements.

3. Results and Discussion

3.1. Single-layer $TiAlC_xN_{1-x}$ coating

Table 1 summarizes the deposition parameters and mechanical properties of single-layer $TiAlC_xN_{1-x}$ coating. The relative concentrations of Ti, Al, C, N were obtained from the XPS analysis. It can be found that the relative content of C increases with the flow rate of CH_4, and the deposition rate increases firstly and then decreases. The deposition rate is linked with the partial pressure of methane, but too much methane will reduce the amount of non-metallic ions (N_2 molecule can supply two N^{3-} ions and CH_4 molecule can only supply one C^{4-} ion).

Fig. 1 shows the surface morphology of single-layer $TiAlC_xN_{1-x}$ coatings, some particles (or microvoids that caused of the flop of metal particles) appear on the samples deposited using the multi-arc-ion-plating technology.[14] The number of particles on $TiAlC_{0.31}N_{0.69}$ coating is the smallest [Fig.1 (c)], and the roughness decreases firstly and then increases with the increase of the partial pressure of methane. In fact, in the plasma, there is a mixture of ions of Ti^{4+}, Al^{3+}, Ar^{+}, H^{+}, N^{3-},

C^{4-}, and electrons as well as melted or unmelted droplets. If CH_4 is introduced, the ionization rate is increased and the metal particles on target surfaces decrease in the temperature that not too high. However, when the flow rate of CH_4 is further increased, the metal particles on the coating surface increase owing to the elevated temperature in the plasma.

As the chemical status of C is one of the decisive factors on hardness and toughness values, XPS analysis result of the C will be analyzed here first. As shown in Fig. 2, the XPS sub-peaks of Ti-C, Al-C, C-C and C-O could be identified from the spectra of $TiAlC_{0.37}N_{0.63}$. Ti-C is indeed a solid-solution hardening phase in the lattice [20]. The coating sample (c) $TiAlC_{0.31}N_{0.69}$ has a higher relative amount of Ti-C, thus it has the maximum hardness (as shown in Fig.3). The relative content of Ti-C in sample (e) $TiAlC_{0.76}N_{0.24}$ is the largest but the hardness is smaller than those of the other samples (b)-(c)-(d). It can be explained with the XRD results as shown in Figure 4 (Grazing Incidence Xray Diffraction, GIXRD). From Fig. 4, samples (a)-(b)-(c)-(d) show the same phase structure as the Ti-Al-N, which indicates that the element C plays a critical role as a dopant in these specimens. However, a different phase structure was detected for sample (e), and in this specimen, the main phase is Ti-(Al)-C and the element N becomes a critical dopant. This indicates that the coatings changes from C-doped Ti-Al-N into N-doped Ti-(Al)-C.

The hardness exhibits the similar trend as that of the toughness, and both the data are listed in Table 1. Figure 5 shows the acoustic emission spectra and scratch morphology of single-layer $TiAlC_xN_{1-x}$ coatings from the scratch adhesion tests. For

TiAlN caoting, there is almost no signal in the spectra and no flaking around the scratch morphology. However, adhesion failure from the acoustic wave signals was observed for all the other coating specimens, and the critical loads corresponding to coating failure are 22 N, 42 N, 53 N and 44 N, respectively for the coatings of $TiAlC_{0.22}N_{0.78}$, $TiAlC_{0.31}N_{0.69}$, $TiAlC_{0.37}N_{0.63}$, and $TiAlC_{0.76}N_{0.24}$ [21]. It shows that the adhesion strength of the TiAlN coating decreases with increase in the C doping concentration, which might be linked to the deteriorated toughness. The $TiAlC_{0.37}N_{0.63}$ coating has the highest binding force of 53 N in samples (b-e), and the failure is particulate (punctiform) flaking rather than scale (sheet) flaking.

Figure 6 shows the friction and wear curves of TiAlN and $TiAlC_xN_{1-x}$ coatings [22]. The coefficient of friction (COF) decreases firstly and then increases with the increases of carbon content, and $TiAlC_{0.37}N_{0.63}$ coating exhibits the lowest friction coefficient and wear rate (as listed in table 1).

The values of the H^3/E^2 ratio[23], which is related to the contact yield pressure of hard coatings, have been calculated and the data are listed in Table 1. It is clear that the variation trend of H^3/E^2 factor is consistent with that of COF curves and wear rate. In fact, the best tribological property occurs in the coating of $TiAlC_{0.37}N_{0.63}$ coating, which also has a high hardness (38.34 GPa), high C-C content (6.8 at.%), good toughness and low elastic modulus (299.09 GPa).

3.2. Multilayer TiAlN/$TiAlC_{0.37}N_{0.63}$ coatings

Based on the above results, the $TiAlC_{0.37}N_{0.63}$ coating exhibits the optimized

tribological behavior, and was then used as a sub-layer for multilayer coatings. Table 2 summarizes some characterization parameters for the multilayer TiAlN/$TiAlC_{0.37}N_{0.63}$ coatings. The thicknesses of sub-layers were determined from the cross-sectional SEM images as shown in Fig. 7. The average deposition rate of TiAlN sub-layer and $TiAlC_{0.37}N_{0.63}$ sub-layer is 17 nm/min and 34 nm/min, respectively. As shown in Fig.7, the layered structure can be visibly identified, although the contrast is not great due to the small elemental difference in two sub-layers (C and N). The modulation period was estimated by averaging the thickness of 5 layers, and the calculated values are 51 nm, 68 nm, and 85 nm respectively. The overall deposition time of the multilayer is 120 min, 135 min, 144 min, respectively.

For nano-indentation, the samples must be in the polished state (Ra≤50 nm) [24], thus the hardness of multilayer coatings with 3.5 μm in thickness cannot be accurately evaluated by the method. The composite hardness of the multilayer coatings on the HSS substrates was tested by Vickers microhardness instrument. The hardness of all the samples is roughly at the same level and the highest one is sample 34nm-34nm.

Figure 8 shows the XRD patterns of multilayer coatings, and those of single-layer TiAlN and $TiAlC_{0.37}N_{0.63}$ are presented as well for comparisons. For samples of 17nm-34nm and 34nm-34nm, a new diffraction peak of TiN_x phase appears as a result of the incomplete nitridation in the interface of TiAl buffer layer and TiAlN transition layer. The single-layer patterns were obtained using GIXRD, and the diffraction peaks of TiN (fcc) phase can be linked to single-layer coatings as

marked in Fig. 8. When the thickness of TiAlN sub-layer is increased to 51 nm, the preferred TiN (111) orientation appears and the peak shifts towards small angle direction.

Fig.9. shows acoustic emission spectra and scratch morphology of multilayer coatings. It is worth noted that no apparent particulate flaking or scale flaking were found in all multilayer coatings. Obviously, both the composite strength and toughness are increased through the multilayer design principle. The sample with a modulation ratio of 1:1(34nm-34nm) and a modulation period of 68 nm has the highest critical load of 52 N.

Fig. 10 shows the friction and wear curves of multilayer coatings, the friction coefficient of samples Ma (17nm-34nm), Mb (34nm-34nm) and Mc (51nm-34nm) is 0.62, 0.46 and 0.70, respectively. The wear rates of the TiAlN/$TiAlC_{0.37}N_{0.63}$ Multilayer coatings are summarized in Table 1, in which sample Mb (34nm-34nm) coating has the lowest wear rate.

3.3 Discussion

The introduction of C in TiAlN results in: (1) the substitutional solid solution, (2) formation of the C-C bond; (3) formation of various carbides, such as TiC, AlC, and carbonitrides of TiCN, AlCN, etc. The flow rates of reaction gases of nitrogen and methane can be changed to tune the hardness, toughness, and wear resistance. The optimum property of single-layer $TiAlC_xN_{1-x}$ was obtained by using a suitable flow ratio of reaction gas (nitrogen: 35sccm, methane: 35sccm). Through the multiple nano-layer designs, multilayer coatings with an appropriate modulation period and

modulation ratio can not only combine the advantages of the sub-layers, but also introduce the interfaces which prevent the slipping of dislocations and crack propagation, and reduce stress concentration [25]. The TiAlN and $TiAlC_{0.37}N_{0.63}$ sub-layers present the same texture (fcc, a=4.24Å, see Fig.8) and a similar elastic modulus (304.22GPa, 299.09GPa, respectively, see table 1). Sample Mb (34nm-34nm) possesses a symmetrical structure[26] (modulation ration=1:1) that can neutralize the stresses in interfaces effectively. By combination of various effects from the above reasons, the hardness, adhesive strength and wear resistance of sample Mb (34nm-34nm) is the best.

4. Conclusions

A series of $TiAlC_xN_{1-x}$ single-layer coatings were prepared by multi-arc ion plating, the doped carbon results in higher hardness, lower toughness, and lower friction coefficient. The $TiAlC_{0.37}N_{0.63}$ coating exhibited the optimized performance, the hardness is 38.34 GPa, the elastic modulus is 299.09 GPa, the factor H^3/E^2 is 0.63 and the room temperature coefficient of friction is 0.53. Accordingly, TiAlN/$TiAlC_{0.37}N_{0.63}$ multilayer coatings were designed to improve the toughness and wear resistance. The results showed that the multilayer coatings with a modulating ratio of 1:1 and a modulation period of 68 nm have a hardness of 2793.9 $HV_{0.10}$, an excellent bonding strength of 52 N and the minimum friction coefficient of 0.46.

Acknowledgements

This work was supported by the National Natural Science Foundation of China (Grant No. 51071119, 51101081, 51271139, 51471130, 51371136), Fundamental Research Funds for the Central Universities.

References

1. J. Musil,2000, 'Hard and superhard nanocomposite coatings', *Surface and Coatings Technology*, **125**(1-3), 322-330.
2. Z. Shouyu and K. Dejun, 2017, 'Microstructures and Friction–Wear Behaviors of Cathodic Arc Ion Plated Chromium Nitride Coatings at High Temperatures', *Journal of Tribology*, **140**(3), 031602.
3. R. Rachbauer, J. J. Gengler, A. A. Voevodin, K. Resch, and P. H. Mayrhofer, 2012, 'Temperature driven evolution of thermal, electrical, and optical properties of Ti-Al-N coatings', *Acta materialia*, **60**(5), 2091-2096.
4. F. Cai, S. Zhang, J. Li, Z. Chen, M. Li, and L. Wang, 2011, 'Effect of nitrogen partial pressure on Al–Ti–N films deposited by arc ion plating', *Applied Surface Science*, **258**(5), 1819-1825.
5. W. Zhou, J. Liang, F. Zhang, J. Mu, and H. Zhao, 2014, 'A comparative research on TiAlN coatings reactively sputtered from powder and from smelting TiAl targets at various nitrogen flow rates', *Applied Surface Science*, **313**, 10-18.
6. L. Chen, Y. X. Xu, Y. Du, and Y. Liu, 2015, 'Effect of bilayer period on structure, mechanical and thermal properties of TiAlN/AlTiN multilayer coatings', *Thin Solid Films*, **592**, 207-214.
7. Y. Zeng, Y. Qiu, X. Mao, S. Tan, Z. Tan, X. Zhang, J. Chen, and J. Jiang, 2015, 'Superhard TiAlCN coatings prepared by radio frequency magnetron sputtering', *Thin Solid Films*, **584**, 283-288.
8. L. Chen, L. He, Y. Xu, L. Zhou, F. Pei, and Y. Du, 2014, 'Influence of ZrN on oxidation resistance of Ti–Al–N coating', *Surface and Coatings Technology*, **244**, 87-91.
9. A. Miletić, P. Panjan, B. Škorić, M. Čekada, G. Dražič, and J. Kovač, 2014, 'Microstructure and mechanical properties of nanostructured Ti–Al–Si–N coatings deposited by magnetron sputtering', *Surface and Coatings Technology*, **241**, 105-111.
10. F. Fernandes, A. Loureiro, T. Polcar, and A. Cavaleiro, 2014, 'The effect of increasing V content on the structure, mechanical properties and oxidation resistance of Ti–Si–V–N films deposited by DC reactive magnetron sputtering', *Applied Surface Science*, **289**, 114-123.
11. S. Veprek, M. G. J. Veprek-Heijman, P. Karvankova, and J. Prochazka, 2005, 'Different approaches to superhard coatings and nanocomposites', *Thin Solid Films*, **476**(1), 1-29.
12. J. Musil and M. Jirout, 2007, 'Toughness of hard nanostructured ceramic thin films', *Surface and Coatings Technology*, **201**(9-11), 5148-5152.
13. S. Zhang, D. Sun, Y. Fu, and H. Du, 2005, 'Toughening of hard nanostructural thin films: a critical review', *Surface and Coatings Technology*, **198**(1-3), 2-8.
14. Z. Zhou, W. M. Rainforth, D. B. Lewis, S. Creasy, J. J. Forsyth, F. Clegg, A. P. Ehiasarian, P. E. Hovespian, and W. D. Münz, 2004, 'Oxidation behaviour of nanoscale TiAlN/VN multilayer coatings', *Surface and Coatings Technology*, **177-178**, 198-203.
15. A. P. Kulkarni and V. G. Sargade, 2015, 'Characterization and Performance of AlTiN, AlTiCrN,

TiN/TiAlN PVD Coated Carbide Tools While Turning SS 304', *Materials and Manufacturing Processes*, **30**(6), 748-755.

16. H. Shang, J. Li, and T. Shao, 2014, 'Mechanical properties and thermal stability of TiAlN/Ta multilayer film deposited by ion beam assisted deposition', *Applied Surface Science*, **310**, 317-320.
17. M. Sakurai, T. Toihara, M. Wang, W. Kurosaka, and S. Miyake, 2008, 'Surface morphology and mechanical properties of nanoscale TiAlN/SiNx multilayer coating deposited by reactive magnetron sputtering', *Surface and Coatings Technology*, **203**(1-2), 171-179.
18. B. Alemón, M. Flores, C. Canto, E. Andrade, O. G. de Lucio, M. F. Rocha, and E. Broitman, 2014, 'Ion beam analysis, corrosion resistance and nanomechanical properties of TiAlCN/CNx multilayer grown by reactive magnetron sputtering', *Nuclear Instruments and Methods in Physics Research Section B: Beam Interactions with Materials and Atoms*, **331**, 134-139.
19. C. S. Jang, J.-H. Jeon, P. K. Song, M. C. Kang, and K. H. Kim, 2005, 'Synthesis and mechanical properties of TiAlCxN1−x coatings deposited by arc ion plating', *Surface and Coatings Technology*, **200**(5-6), 1501-1506.
20. X. Zhang, J. Jiang, Z. Yuqiao, J. Lin, F. Wang, and J. J. Moore, 2008, 'Effect of carbon on TiAlCN coatings deposited by reactive magnetron sputtering', *Surface and Coatings Technology*, **203**(5-7), 594-597.
21. S. Zhang, L. Wang, Q. Wang, and M. Li, 2013, 'A superhard CrAlSiN superlattice coating deposited by a multi-arc ion plating: II. Thermal stability and oxidation resistance', *Surface and Coatings Technology*, **214**, 153-159.
22. X. Zhang, Y. Qiu, Z. Tan, J. Lin, A. Xu, Y. Zeng, J. J. Moore, and J. Jiang, 2014, 'Effect of Al content on structure and properties of TiAlCN coatings prepared by magnetron sputtering', *Journal of Alloys and Compounds*, **617**, 81-85.
23. M. A. Al-Bukhaiti, K. A. Al-hatab, W. Tillmann, F. Hoffmann, and T. Sprute,2014, 'Tribological and mechanical properties of Ti/TiAlN/TiAlCN nanoscale multilayer PVD coatings deposited on AISI H11 hot work tool steel', *Applied Surface Science*, **318**, 180-190.
24. L. Wang, S. Zhang, Z. Chen, J. Li, and M. Li, 2012, 'Influence of deposition parameters on hard Cr–Al–N coatings deposited by multi-arc ion plating', *Applied Surface Science*, **258**(8), 3629-3636.
25. M. Pfeiler-Deutschmann, P. H. Mayrhofer, K. Chladil, M. Penoy, C. Michotte, M. Kathrein, and C. Mitterer, 2015, 'Effect of wavelength modulation of arc evaporated Ti–Al–N/Ti–Al–V–N multilayer coatings on microstructure and mechanical/tribological properties', *Thin Solid Films*, **581**, 20-24.
26. Z. Lei, Y. Liu, F. Ma, Z. Song, and Y. Li, 2016, 'Oxidation resistance of TiAlN/ZrN multilayer coatings', *Vacuum*, **127**, 22-29.

Figures and Tables

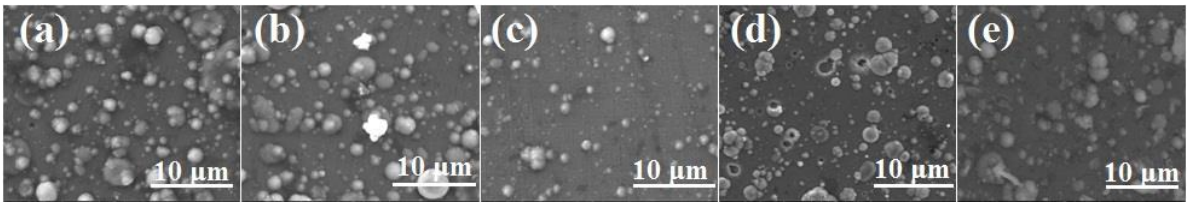

Fig.1. SEM images of surface morphology of TiAl(C)N coatings: (a) TiAlN, (b) $TiAlC_{0.22}N_{0.78}$, (c) $TiAlC_{0.31}N_{0.69}$,(d) $TiAlC_{0.37}N_{0.63}$, (e) $TiAlC_{0.76}N_{0.24}$.

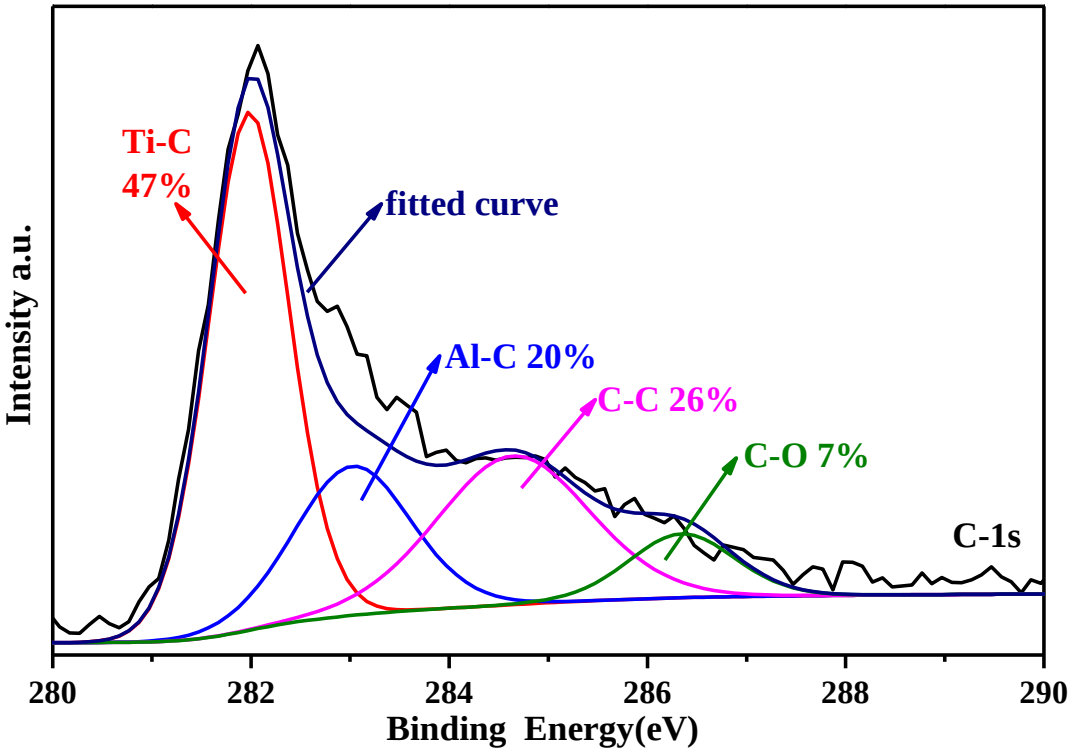

Fig.2. XPS spectra of C-1s in $TiAlC_{0.37}N_{0.63}$ coating, C-C will have both SP2 and SP3,

C-O is surface adsorption

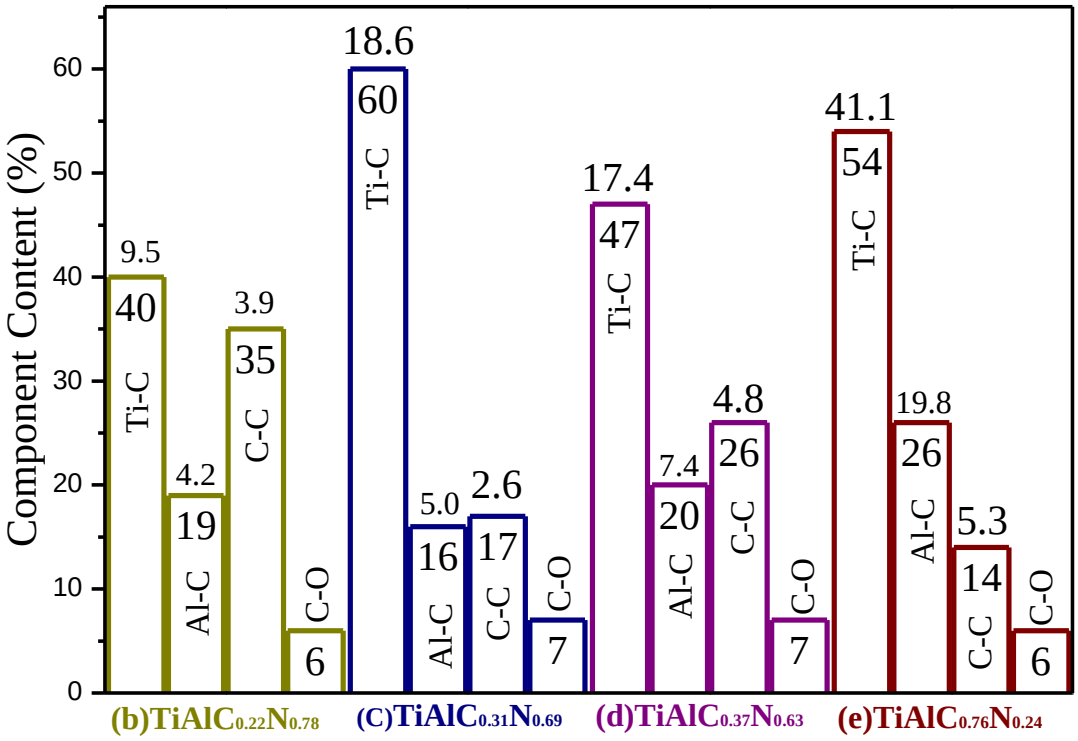

Fig.3. Binding status of C in $TiAlC_xN_{1-x}$ coatings obtained by XPS.

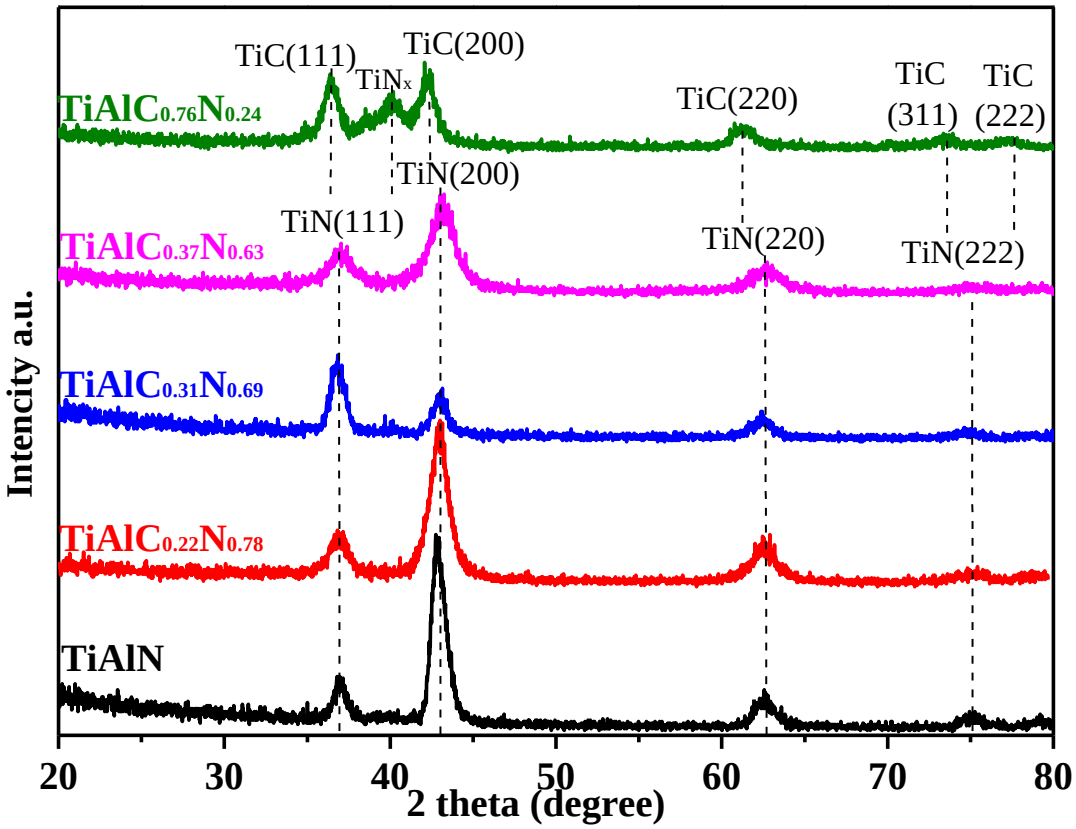

Fig. 4. XRD patterns of $TiAlC_xN_{1-x}$ coatings.

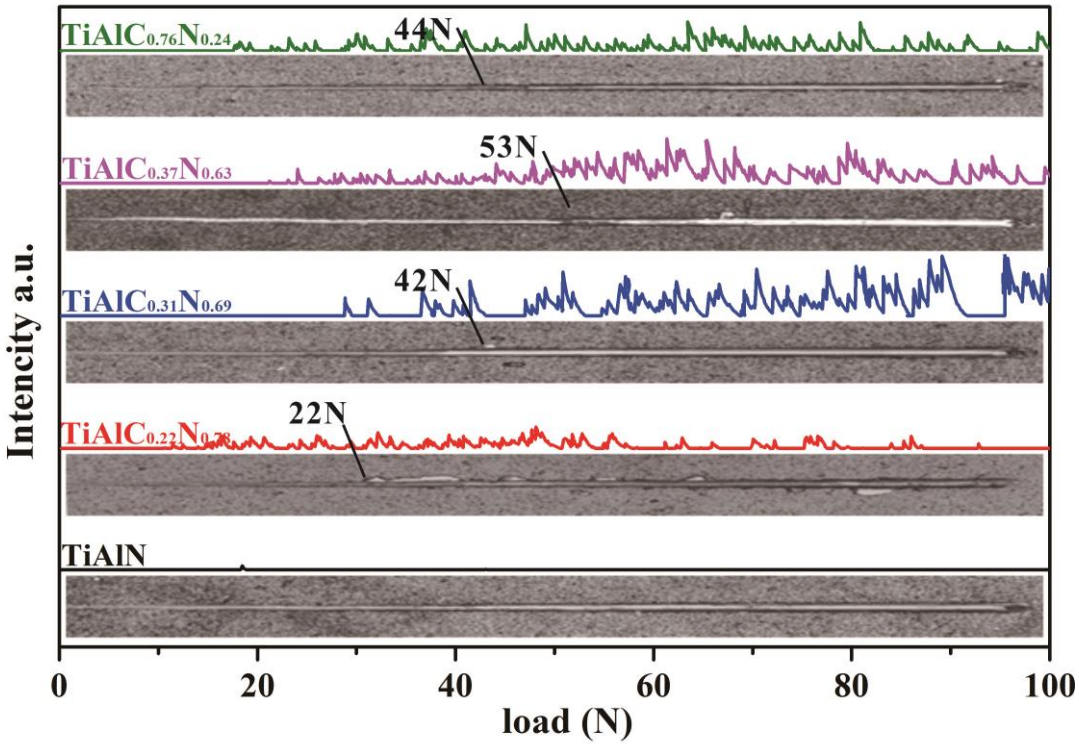

Fig. 5. Acoustic emission spectra and scratch morphology of $TiAlC_xN_{1-x}$ coatings.

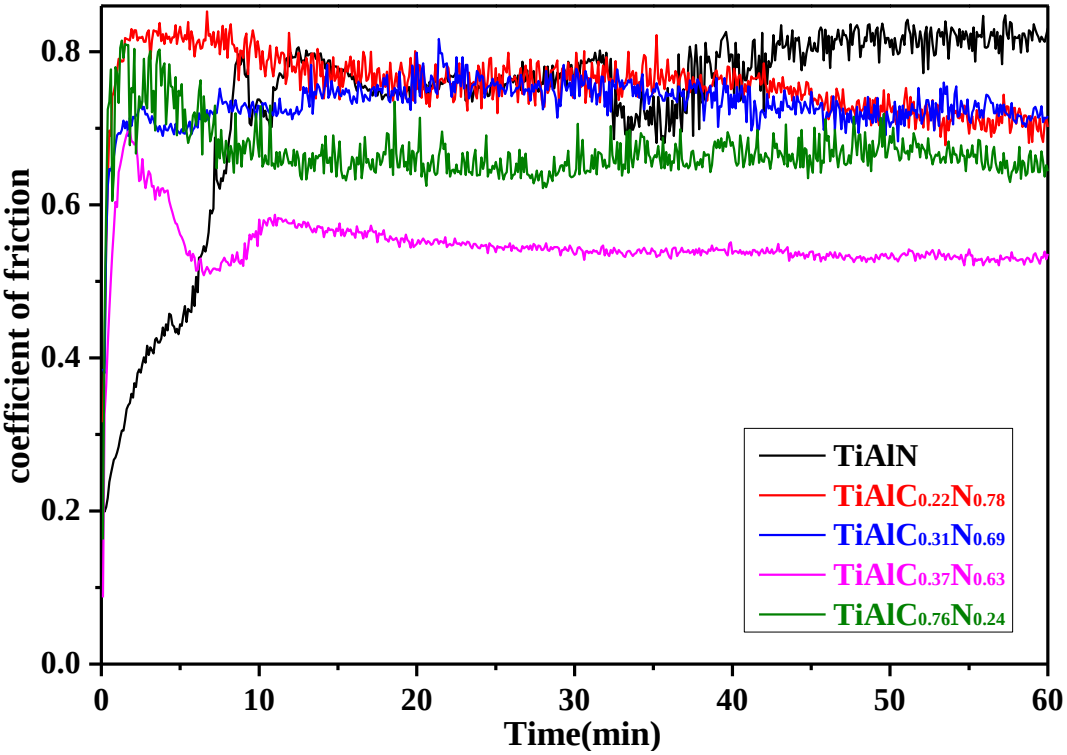

Fig. 6. Friction coefficient versus loading time of $TiAlC_xN_{1-x}$ coatings tested by the pin-on-disk method with the load of 3N.

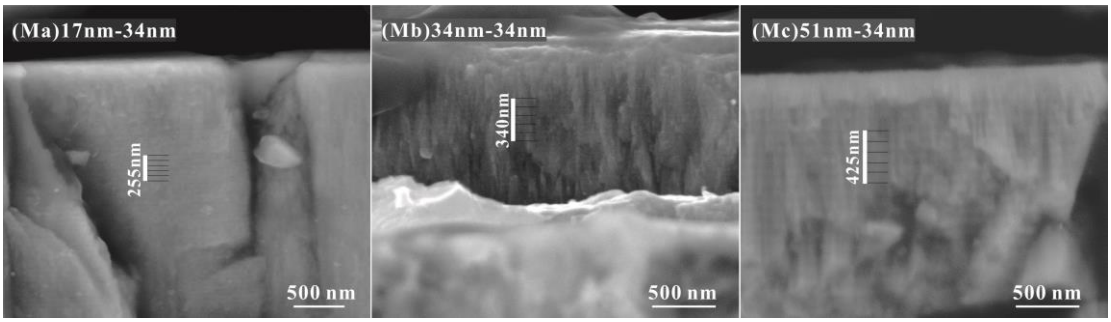

Fig. 7. Cross-sectional SEM images of TiAlN/TiAl$C_{0.37}N_{0.63}$ multilayer coatings.

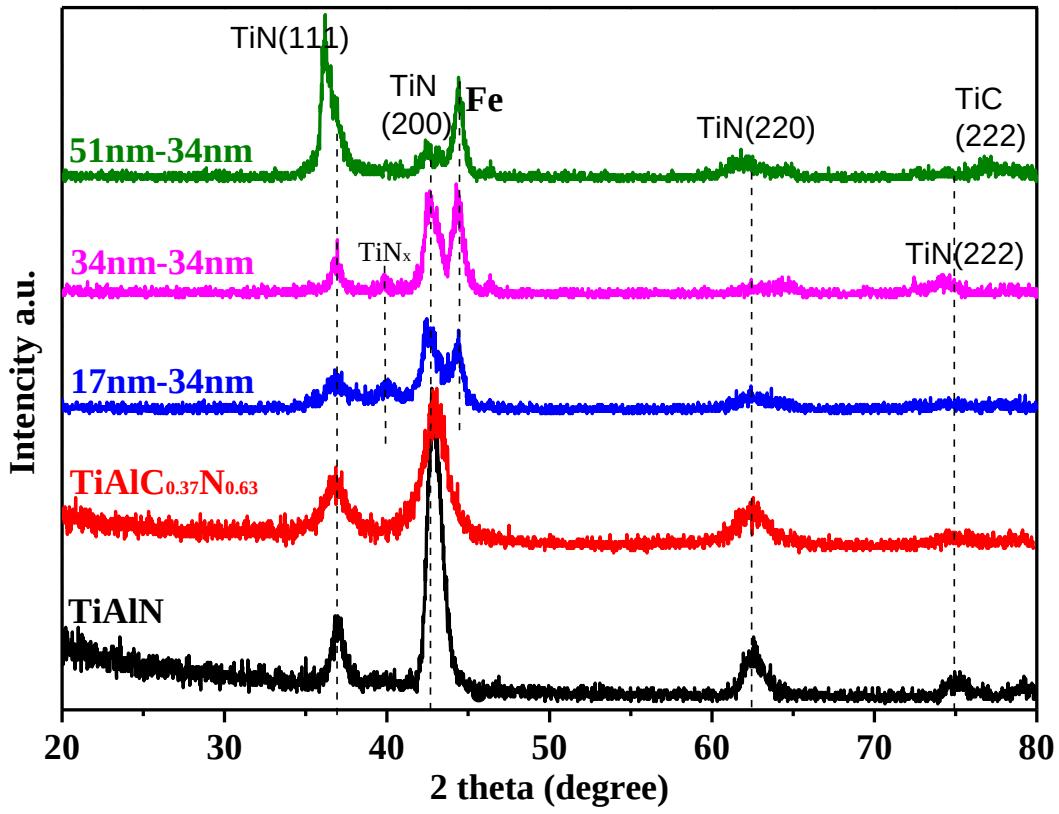

Fig. 8. XRD patterns of TiAlN/TiAl$C_{0.37}N_{0.63}$ multilayer coatings.

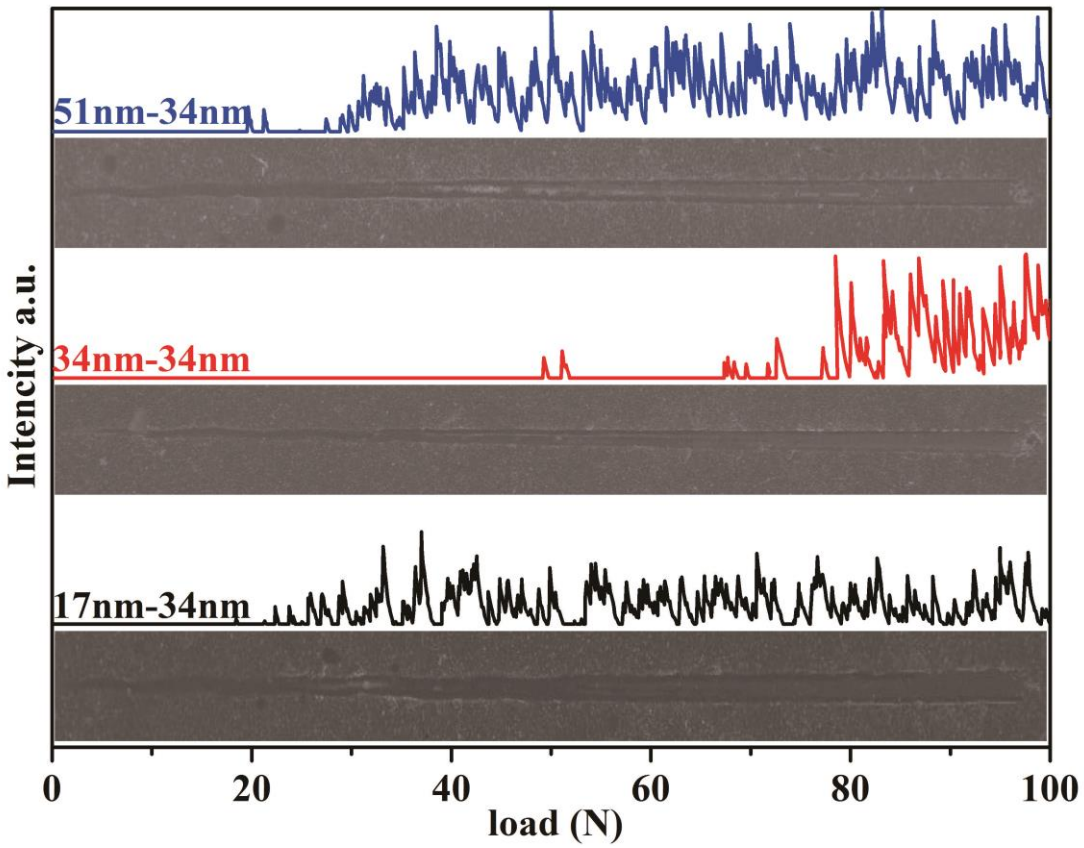

Fig. 9. Acoustic emission spectra and scratch morphology of multilayer coatings.

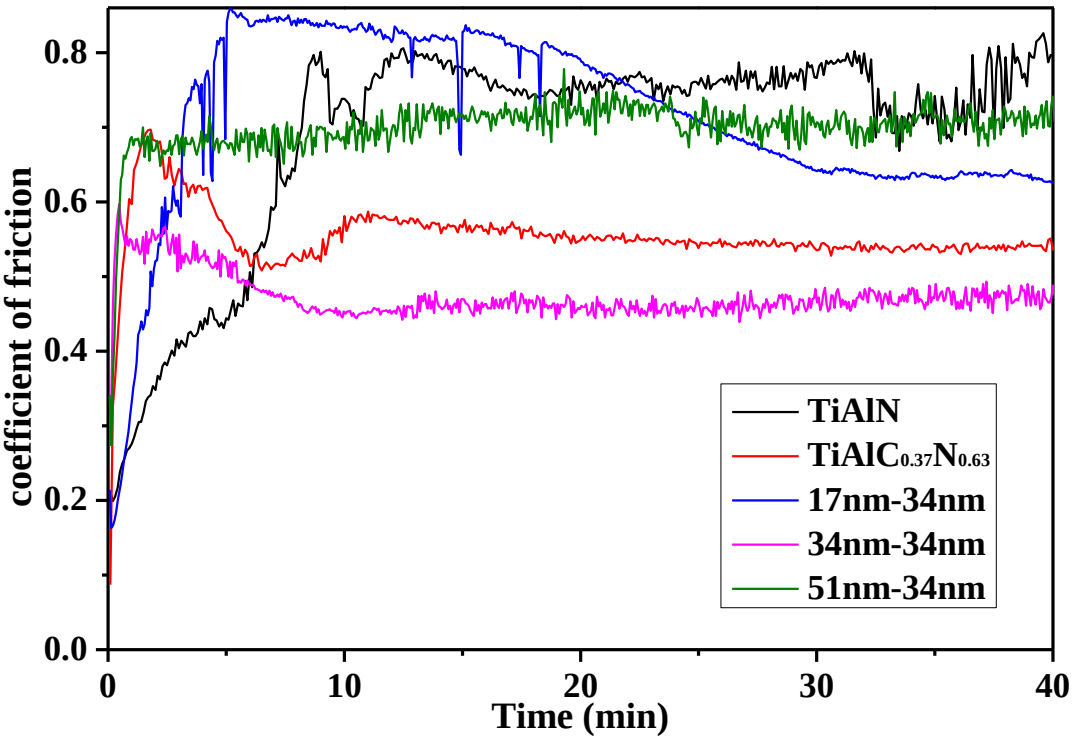

Fig. 10. Friction coefficient versus loading time of multilayer coatings.

Table 1. Deposition conditions and mechanical and tribological properties of coatings obtained by multi-arc-ion plating.

Sample designation	**N_2 (sccm)**	**CH_4 (sccm)**	**Thickness (μm)**	**Hardness (GPa)**	**Elastic Modulus (GPa)**	**H^3/E^2**	**Wear Rate ($mm^3/N·m$)**
TiAlN	70	0	3.4	36.55	304.22	0.53	4.37×10^{-4}
$TiAlC_{0.22}N_{0.78}$	55	15	3.8	37.94	319.68	0.54	2.33×10^{-4}
$TiAlC_{0.31}N_{0.69}$	45	25	4.3	40.38	338.40	0.58	9.05×10^{-5}
$TiAlC_{0.37}N_{0.63}$	35	35	6.7	38.34	299.09	0.63	4.54×10^{-5}
$TiAlC_{0.76}N_{0.24}$	20	50	5.2	37.85	299.04	0.61	6.26×10^{-5}

Table 2. Deposition Deposition conditions and mechanical and triological properties of $TiAlN/TiAlC_{0.37}N_{0.63}$ Multilayer coatings.

Sample designation	**TiAlN (s-nm)**	**$TiAlC_{0.37}N_{0.63}$ (s-nm)**	**Modulation period**	**Thickness (μm)**	**Hardness ($HV_{0.10}$)**	**Wear Rate ($mm^3/N·m$)**
17nm-34nm	60s-17nm	60s-34nm	51 nm×60	3.06+0.5	2677.7	6.34×10^{-5}
34nm-34nm	120s-34nm	60s-34nm	68 nm×45	3.06+0.5	2793.9	1.45×10^{-5}
51nm-34nm	180s-51nm	60s-34nm	85 nm×36	3.06+0.5	2609.4	5.22×10^{-5}